NAL Proposal No: 0131

Correspondents: David H. Miller,
Dieter Cords
Department of Physics
Purdue University
Lafayette, Ind. 47907

FTS/off-net: (317) 633-7000
749-2961

NAL BUBBLE CHAMBER PROPOSAL

K^-p and $\bar{p}p$ Interactions at 200 GeV

We propose to study K^-p and $\bar{p}p$ interactions at 200 GeV in the hydrogen filled NAL 30" bubble chamber with a supplementary visual spectrometer. We request 200,000 pictures. This exposure is intended as a follow up experiment to our proposal "Multiparticle π^-p Interactions at 130 GeV and at the Highest Energy" of April 23, 1971.

Purdue High Energy Physics Group

V. E. Barnes, D. D. Carmony, R. S. Christian, E. C. Fowler, J. A. Gaidos, A. F. Garfinkel, L. J. Gutay, S. Lichtman, F. J. Loeffler R. L. McIlwain, D. H. Miller, T. R. Palfrey, Jr., R. B. Willmann, D. Cords, J. Lamsa, K. Paler, K. Rangan, J. H. Scharenguivel.

April 28, 1971

I. Operation of the Experimental Set-up.

The experimental arrangement is discussed in detail in section IV. Here we are mainly concerned with the feasibility of this experimental proposal, in order to justify section II on the expected and unexpected physics involved.

1. Particle ratios in the beam and event rates

The highest momentum primary proton beam is required at the secondary target in order to obtain a large $\frac{K^- + \bar{p}}{\pi^-}$ ratio. For 500 GeV pp collisions we have studied the variation of the ratio $\frac{K^- + \bar{p}}{\pi^-}$ with the secondary momentum and the production angle. We used the Hagedorn-Ranft model[1,2] for semi-emperical predictions. According to the authors the model is more reliable in predicting the particle ratios than the particle yields.

In fig. 1 we have plotted the π^- yield at the target versus the ratios $\frac{K^-}{\pi^-}$ and $\frac{\bar{p}}{\pi^-}$ at the bubble chamber (1000 m beam length have been taken into account). The solid curves represent secondary momenta starting at 150 GeV and increasing in steps 50 GeV and the dashed lines are production angles starting at 0 degree and increasing in steps of .1 degree. Since the ratios $\frac{K^-}{\pi^-}$ and $\frac{\bar{p}}{\pi^-}$ are increasing with increasing production angle, we select the negative beam at a fairly high production angle: 0.5 degree or 8.7 mrad for the proposed secondary momentum of 200 GeV (see circles in fig. 1). We conclude from the NAL beam report by Lach and Pruss[3] that such a large production angle is possible. (The 30" beam line views the target at 3 mrad and the target magnet allows a further deflection up to 3 mrad at 500 GeV or 7.5 mrad at 200 GeV.) From fig. 1 we see that at an angle of .5 degree and a secondary momentum of 200 GeV the ratios $\frac{K^-}{\pi^-}$ and $\frac{\bar{p}}{\pi^-}$ are 12% in both cases. In other words, under these specifications the negative beam consists of 10% K^- and 10% $\bar{p}$.

These high ratios together with a decent particle flux at the bubble chamber can be achieved only by a sharp increase in the primary beam intensity. One can see from the vertical scale in fig. 1 that - going from 0 to 0.5 degree production angle - the primary proton intensity has to be increased by a factor of 3200 to obtain the same secondary particle flux. For a 0.5 degree production angle, an angular acceptance of 0.3 μsr, and a momentum bite of 0.1% $\frac{\Delta p}{p}$ we get 20 particles at the bubble chamber if, according to the NAL beam report[3], $5*10^{10}$ † protons hit the beryllium target at 500 GeV.

Provided that this is feasible and that the above considerations are correct, we would get from 20 negative tracks $2K^-$ and $2\bar{p}$ per expansion. Assuming 20 mb K^- and 40 mb $\bar{p}$ total cross sections the exposure of 200,000 pictures would yield 11,000 K^-p and 22,000 $\bar{p}p$ interactions inside a fiducial volume of 15".

Using the Hagedorn-Ranft calculations for pp collisions at 500 GeV can at this stage be only a best guess. Should the experimental findings contradict seriously these calculations the present proposal has to be reconsidered.†† Using pp instead of p beryllium collisions should have a minor effect. The main difference comes from the absorption inside the beryllium nucleus and would probably lead to a higher $\frac{K^-}{\pi^-}$ and a lower $\frac{\bar{p}}{\pi^-}$ ratio than obtained above, because of the different total cross sections.

---

† Provided momentum tagging is possible one could allow for the maximum possible momentum bite of 0.6% $\frac{\Delta p}{p}$, and bring the beam intensity down to 10^{10} protons per exposure.

†† Results from our preceeding π^-p proposal of April 23 with tagged K^- and $\bar{p}$ particles at 130 GeV may serve to check the Hagedorn-Ranft predictions.

In case protons at 500 GeV would not be available or, if available, the intensity of 10^{10} protons per exposure could not be reached, the choice of a smaller momentum of the negative beam has to be considered.

2. Hardware considerations

We intend to run the bubble chamber in an untriggered mode. In addition to the 33,000 events inside the fiducial volume, nearly twice as many events are expected in the rest of the chamber and in the chamber windows which gives a total of approximately 100,000 events. A trigger on these events could save us taking 100,000 more pictures, but it could easily introduce a serious bias in the event selection, especially if one looks for new or unexpected phenomena. We therefore decide to apply no trigger to the bubble chamber flash.

The requirements for the beam are outlined in part 2 of Section IV. A second beam Cerenkov counter is really needed to tag K^- and $\bar{p}$, and a fast kicker is highly desirable in view of the high flux of 20 particles per exposure. We would, in fact, trigger the kicker on 20 incoming tracks or on a K^- (or $\bar{p}$) interaction detected in the combined upbeam-downstream logic, whichever condition is satisfied first.

The supplementary visual spectrometer consists of wide-gap optical spark chambers and a bending magnet. Its arrangement and its effect on the resolution are described in part 3 of Section IV. The trigger for the spark chambers has to be gated with a signal from the first Cerenkov counter which discriminates π^- from heavier particles.

II. Physics Justification

1. Inclusive Studies

Distributions of one or several particles can be studied - irrespective of the specific reactions involved - in an average sense. Such inclusive studies have been proposed in the context of the thermodynamic model of Hagedorn and Ranft,[1] the parton model of Feynman,[4] the limiting fragmentation of Benecke et al.,[5] and the idea of pionization of Bali et al.[6] Comparisons with experiments and investigations as to scaling laws, factorization properties and limiting distributions have been started in recent years.[2,7,8,9,10,11]

An interesting check for the above-mentioned theoretical ideas is the pair production in $\bar{p}p$ collisions. At least the thermodynamic model predicts a strong suppression for the production of heavy pairs like quarks, and as Hagedorn[12] has shown recently, his ideas are to a certain extent equivalent to the parton model and the limiting fragmentation. Therefore the observation or non-observation of heavy pairs would test the assumption involved.

2. Diffraction Dissociation

A step towards the analysis of specific reactions would be the investigation of the diffraction dissociation of the projectile and/or the target which is expected[13] to dominate Reggeized particle exchanges at 200 GeV. At present energies of 20 GeV the study of diffraction dissociation is limited to small changes in the mass of the dissociating object, since it has been noted[14] that a certain "threshold" for diffraction dissociation has to be overcome:

$$p_{inc} \gg p_{thresh} = \frac{M^{*2} - M^2}{2m_\pi}$$

where p_{inc} is the incident momentum and M and M^* are the masses before and after dissociation. At 200 GeV the change in mass can extend over several GeV.

As has been noted in our previous proposal on multiparticle $\pi^- p$ interactions (April[23], 1971) the target proton dissociation can be studied in detail,

since the decay products will be slow in the laboratory and therefore well measured. Because of the preferred small momentum transfer the beam particle will be measured in the downstream spectrometer.

The projectile dissociation can be studied in a less direct way by measuring the intermediate-range recoil protons in the bubble chamber. However, the resolution for states of mass M is fairly poor,[15]

$$\Delta M = .4/M \text{ (GeV)}$$

at 200 GeV incident energy.

A substantial class of events in general will have the leading proton identifiable, including elastic events, but not including very high multiplicity events.[16]

3. Elastic Scattering

Elastic scattering may be of interest for bubble chamber analyses until counter experiments cover this part of physics with high precision. At 200 GeV it is much easier for the bubble chamber to identify a slow proton than for a counter set-up to identify a secondary meson or nucleon with a momentum close to 200 GeV. The event rate at 200 GeV is expected to be still of the order of 10% of the total cross section. Even if the momentum of the fast outgoing track is only badly determined, a 4c fit should be able to pick out the right class of events.

Besides determining the cross section and the slope of $d\sigma/dt$ it would be of interest to find the order of magnitude of the real part of the amplitude. From experiments below 30 GeV and from model predictions[17,18] it is expected that the real parts are zero for meson-nucleon and $\bar{p}p$ scattering.

4. Hyperon Production and Unexpected Phenomena

Since the hypercharge of the K^-p and $\bar{p}p$ systems is zero, the production of

a wide range of strange particles is observed at present energies and can also be expected at the soon available higher energies. For $\bar{p}p$ collisions the cross section for strange particle production, which goes mainly via hyperon-antihyperon production, is of the order of 2% of the total cross section for incident momenta around 10 GeV.[19] Since the rapid decrease of the total $\bar{p}p$ cross section is thought to be mainly due to the strongly decreasing annihilation cross section, the strange particle production may hold up at higher energies and be ~~of~~ a few percent at 200 GeV.

The rarest particles Ω^- and $\bar{\Xi}^-$ have been found in K^-p and $\bar{p}p$ collisions. Therefore, one may hope to find further interesting or unexpected phenomena in these interactions, expecially when the incident beam momentum is increased by an order of magnitude. Should Ω^- and Ξ^- particles be produced in some appreciable amount one can look for and investigate their secondary interactions.

Target-like hyperon production can be studied with relatively good precision for the same reasons that applied to target proton dissociation in section 2. For decaying neutral particles and for the detection of odd events the down-stream spectrometer is an extremely useful tool.

5. Supplementary Comments

Information on the production of neutral pions is desirable for the following reasons:

a) the inclusive studies of section 1 can be supplemented by the knowledge of the multiplicity and approximate average distributions of π^0's

b) many strange particle decays include π^0's. Therefore the analysis of target-like hyperon production will yield more information if π^0's are detected.

c) the observation of unexpected phenomena may be aided.

Part of this information is supplied by the shower spark chambers at the far

end of the downstream spectrometer, at least when energetic forward-going γ's are involved.

In order to obtain a more comprehensive knowledge on π^o and γ production we intend to propose an experiment with the heavy liquid-filled 30" bubble chamber at a later stage.

III. Analysis Capability

We plan to make a fast scan for unusual phenomena. In addition to the 7 scanning machines in operation at Purdue in Lafayette, there are 2 scanning machines at Purdue in Indianapolis. Measurements will be of high accuracy and quality using the Purdue POLLY-type machine which will be capable of measuring 4000 events per week.

IV. Experimental Arrangement for the Proposed 30-inch Bubble Chamber - Optical Spark Chamber Hybrid System

The main components of the proposed detector system are shown in Figure 1. These include:

(1) The 30-inch hydrogen bubble chamber, for observation of the interaction vertex and analysis of all low energy charged particles with momenta below ∿20 GeV/c.

(2) An upstream beam diagnostic system for providing precise measurements of beam particles.

(3) A wide gap optical spark chamber spectrometer situated downstream for providing important additional data on energetic secondary charged particles with momenta above approximately 20 GeV/c.

(4) A shower spark chamber system situated behind the spectrometer for information on very energetic gamma rays.

While the arrangement is similar in some respects to the bubble chamber - spark chamber detector system described in the Aspen study of Fields, et al.[1], it is not required for the present initial experiment to have the very high accuracy requirements for final state fitting which was of primary interest in the latter study.

These components are matched to the kinematic requirements, as discussed below, in such a way that they provide relatively complete examination of individual multiparticle interactions in the 100 GeV/c region and above. The most noticeable feature of multiparticle interactions as presently known is the tendency for the emitted particles to be produced with relatively small transverse momenta. Those going backwards in the cm system with large longi-

tudinal momenta then appear in the laboratory system with low momenta and large angles. Particles with small longitudinal momenta can appear in the lab at intermediate momenta and angles, while the forward particles in the cm appear as highly collimated, energetic components of a forward jet.

Examples of kinematically allowed regions for transverse and longitudinal cm momenta are shown in the Peyrou plot of Figure 2 for the case of 500 GeV/c πp interactions. Superposed are the expected contours for laboratory angles and momenta of outgoing pions, showing the characteristics described above. For greater detail, the region of small transverse momenta is shown in Figure 3. Backward pions in the cm with transverse momenta below 1 GeV/c are seen to have laboratory momenta of less than $\sim$20 GeV/c, and can appear at angles even beyond 90°.

Similar behavior is illustrated for secondary protons from 200 GeV/c pp interactions in Figure 4, except that the allowed maximum laboratory angle here must be less than 90°. On the other hand, those particles produced with small or forward longitudinal momenta P_L, and transverse momenta $P_T \lesssim 1$ GeV/c, are seen to have laboratory momenta above approximately 20 GeV/c and are confined to a forward cone of less than approximately ±4° opening angle.

1. Bubble Chamber

The main bubble chamber requirements here are good track resolution, angular precision $\lesssim$ 1 mrad, good momentum accuracy up to the 20 GeV/c region, and provision of suitable exit windows and magnet apertures for the forward secondaries. The 30-inch bubble chamber is eminently suitable, without requiring any significant modifications.

The gross chamber features illustrated in Figure 1 are those of the 30-inch, whose characteristics include high resolution dark field optics, a

magnetic field of 32 KG, multipulsing capabilities of $\lesssim$ five expansions per 0.5 seconds, and a maximum detectable momentum of over 1000 GeV/c. In the configuration shown in Figure 1, the beam is brought in through a small window which is currently in use as an exit window for a neutral hadron hybrid spectrometer at ANL. The limiting exit angle allowed by the magnet structure in the horizontal plane is confined to approximately ±3.5°, which corresponds to allowing all secondary particles above ∿20 GeV/c to enter the downstream spark chamber spectrometer. In the vertical plane the magnet iron and beam exit windows allow particles at angles up to approximately ±10°. Thus, it is obvious that the analysis of tracks below ∿20 GeV/c will necessarily be performed in the bubble chamber, where $\Delta p/p \lesssim 10\%$ and $\Delta\theta \lesssim 1$ mrad. This, in our opinion, is a satisfactory level of performance for this particular group of produced particles.

2. Bubble Chamber Beam

Since the spectrometer facility is planned to be of general use, a comprehensive beam system is required. This section discusses beam characteristics and beam defining equipment which we regard as necessary to do a variety of experiments in the 30-inch bubble chamber with the associated downstream spectrometer. It is assumed that the beam, as described in the Lach-Pruss report[2], will be constructed, including a secondary hadron target. It is also assumed that fluxes of at least 10^{10} protons will be available at the secondary hadron target, with a spill time between 60 and 200 μ sec. Two or three such spills per accelerator pulse would be highly desirable for bubble chamber multi-pulsing. In addition, it is assumed that beam tuning detectors (scintillators or wire proportional chambers) will exist, and also at least one Cerenkov counter to determine relative fractions of π, K and p.

In addition,

A) it is felt that a flux-limiting fast kicker will permit much more efficient use of the bubble chamber, giving cleaner pictures and avoiding unusable pictures;

B) a Cerenkov counter which can efficiently tag π's vs. (K and p) up to 200 GeV/c is desirable for beam purity in view of possible significant fractions of K^- and $\bar{p}$[2,3];

C) a second Cerenkov counter which can tag (π^-, K^-) vs. $\bar{p}$ will permit studies of K^- and $\bar{p}$ interactions as a by-product of a π^- experiment. Eventually K^- and $\bar{p}$ enrichment triggering might be done. If K^+/p and π^+/p ratios are good, similar arguments will apply for positive beams;

D) position tagging of each beam track in the chamber, in time correlation with the above Cerenkov signals, will be necessary.

E) external determination of beam momentum and angles will be mandatory in most cases. Five small proportional wire chambers can do this job and also tag all beam tracks in (D).

We now discuss items (A) - (E) in greater detail.

A) <u>Fast Flux limiting Beam Kicker</u>

A 1-2 μ sec. kicker with integral $Bdl \cong$ one Kg-m would kick the 5mm high target image upward by 0.065 mrad, or by 13 mm with a 200 meter lever arm. The kicker should be located 1000 feet from the chamber. However, the beam track counter should be placed at the chamber entry window to avoid uncertainty in n. The signal propagation delay ($\sim$2 μ sec.) is comparable to the rise time, plus there are logic and ignition delays. Given a total delay of 4 to 7 μ sec., n = 10 tracks/picture, and 100 μ sec. spill time, one could control the flux to 10%, which is excellent. This is enormously better than

the typical fluctuations without a kicker, and should eliminate a source of wasted bubble chamber photographs and wasted accelerator pulses.

B and C) Cerenkov Tagging of π, K and p

Extrapolations[3] of Serpukhov data indicate that 500 GeV/c protons on a target will produce a rich ratio of K^-/π^- and $\bar{p}/\pi^-$ at 100 GeV/c -- 5% and 15% respectively, 1 km. away at the bubble chamber. The need for π^- tagging in this case is obvious, and the opportunity to study tagged K^- and $\bar{p}$ interactions early is attractive. In secondary positive beams, p and π^+ and probably K^+ will all be present in significant amounts at some energies, and will require tagging.

S. Pruss (NAL) has suggested a differential Cerenkov design, an outgrowth of ideas he presented at the 1970 Summer Study[4]. Small angle light is directed to one phototube and light between this angle and a larger angle is directed to a second phototube. For Cerenkov angles $\sim$5 mrad, the angular separation of π's from K's at 200 GeV/c is several times the natural beam divergence of 10^{-4}mrad, or the chromatic $\Delta\theta$. Good photon fluxes at these angles should permit efficient tagging at p $\lesssim$ 200-250 GeV/c or beyond. A second Cerenkov counter of identical design would then permit separation of p from K and π.

The design involves 40m of Helium-filled pipe at $\sim$.2 to 1 atmosphere absolute, downstream diameter 12" to 18", a 100" focal length spherical mirror, and the above-mentioned phototube array. High counting efficiencies can be obtained even beyond 200 GeV/c in the differential mode of operation with this length. Beam divergence must be $\lesssim$ 0.1 mrad, close to what is achievable in the existing beam design.[2] Pressure must be monitored to 10 mm of mercury and average temperatures to 5°C.

D) Position Tagging of Tracks to Correlate with Cerenkov Information

Minimal position tagging could be accomplished with a crossed pair of picket fence scintillator arrays. This means a non-negligible number of photomultiplier tubes, since the number, m, of x-y resolution elements should be many times greater than the number, n, of beam tracks to reduce the probability of two tracks in one hodoscope location. Moreover, one must record the bubble chamber frame number and x-y for each beam track. Thus, a fast parallel shift register is needed to absorb information during the beam spill and later pass it on to a computer or perhaps directly to an incremental tape unit.

With this in mind, we suggest the use of small proportional wire arrays of 50 to 100 wires, read out as above. One gets greater x-y resolution at somewhat less cost and can also achieve the purposes of item (E). Such a system is illustrated in Figure 5.

E) Angle and Momentum Tagging.

To use the 30" bubble chamber efficiently, one should start the fiducial volume immediately at the beginning of the liquid. Hence, one must know p and θ of the beam externally. In any case, one can do better externally than by measuring short beam tracks in the liquid. From beam optics one will have $\delta\theta \simeq 10^{-4}$ rad and $\delta p/p = 0.066\%$.[2] However, in flux-limited situations one may want to increase the momentum bite to 1%. Then it pays to replace the momentum slit with a proportional wire array and win back the $\delta p/p$ inherent in the target size. This corresponds to a wire spacing of 2mm. A more refined system can be made with 1 mm. wire spacing, but several such chambers would be required to determine orbits better. In effect, the equivalent of a second plane near the target is needed to reduce the "target size". In

this case one also improves upon the .066% which can be achieved with momentum slits.

The phase space of the beam as designed is 10^{-9} inch^2-steradian. With a reasonable beam size in the chamber, for example $\sim$ 0.5 x 3.0 inches, either the beam is parallel to 10^{-4} rad or its angle can be determined to 10^{-4} by measuring position in the chambers. This matches $\delta\theta_{coulomb} \lesssim 10^{-4}$ from the entry windows, and also matches for beam up to 500 GeV/c with the transverse momentum accuracy one obtains from measuring outgoing tracks in the last half of the bubble chamber or better still in the wide gap optical chambers.

To survey the proportional chambers, a well measured non-interacting track in the bubble chamber determines θ to 0.5×10^{-4} in y, and 1.5×10^{-4} in z, while $\delta\theta(\text{coulomb}) \sim 10^{-4}$ from the entry windows. At a distance of 13 m, the wire location is known to 1.5 and 2.4 mm respectively in y and z, from a single track.

We propose to use an existing, tested design of Charpak chamber[5] with good space resolution and immunity to spark chamber noise, compact and with a relatively small number of wires in total. We could certainly put the information onto magnetic tape, together with Cerenkov counter signals, for each beam track into the bubble chamber. Frame numbers would also be written onto the tape between beam pulses. A small computer would be the most flexible readout device. A fast parallel shift register or equivalent will be needed to interface the proportional wire and Cerenkov signals. The computer could in principle be dispensed with and the information written directly from the shift register by an incremental tape unit, but with the loss of online diagnostic capabilities. Given a computer with a fast printer, the track tagging information could be printed out frame by frame for each roll,

avoiding magnetic tape and associated format problems for the users.

3. Spark Chamber Spectrometer

Although many of the salient features of multiparticle interactions will be obtained from the analysis of only the low energy particles seen in the bubble chamber, as illustrated in the previous discussion, we believe that additional insight can be provided by supplementary information on the more energetic downstream components of the same events. The following deals with four important aspects of the system:

(A) spectrometer resolution,

(B) spark chamber optics,

(C) gamma-ray detection and,

(D) trigger schemes.

(A) Spark Chamber Spectrometer Resolution

The apparatus, as shown in Figure 1, includes no external magnetic field other than that of the bubble chamber itself. Calculations show that utilizing (a) the event vertex location in the bubble chamber (b) the chamber's fringing field and (c) track locations in the wide gap chambers a typical $\Delta p/p$ accuracy of ±5-10% or less is readily obtainable for fast secondaries produced in a 200 GeV/c collision on hydrogen. It is clear, however, that considerable additional accuracy is available on the very small angle fast secondaries with the addition of a magnet downstream. Preliminary considerations for such a system are also presented.

In the initial scheme, two spark chamber units are utilized, one immediately behind the bubble chamber magnet with four gaps of active volume 36" wide by 48" high by 8" deep and the other unit 4.5 meters downstream, against

the far wall of the bubble chamber building, with the same dimensions. The downstream 36" dimension subtends a ±3.5° angle from the bubble chamber. Assuming the following parameters: (1) ±500 μ on each point measured in the spark chambers (2) eight points measured per spark chamber unit (3) ±50 μ on the vertex in the bubble chamber and (4) 872 KG-in of integral Bdl in the bubble chamber fringing field we find that $\pm\Delta p/p$ (%) $\simeq$ 0.07 p (GeV/c). Taking into account the following sources of error due to multiple coulomb scattering: (1) 15" of LH_2 (2) 0.12" of Fe (B.C. window) (3) 0.25" of Al (vacuum tank windows) and (4) 0.5 cm of counters and other smaller sources (air, chamber walls), the resultant $\pm\Delta p/p$(%) has been determined and is shown in Figure 6. With the exception of the fastest secondaries produced at the highest momenta proposed, the calculations show that the downstream spectrometer will provide data comparable in accuracy to that of the bubble chamber at lower secondary momenta and permit a complete study, in conjunction with the bubble chamber, of all interesting production angles.

The necessary and straight forward extension of the apparatus to yield more precision in the momentum determination of fast forward particles requires an additional spark chamber module plus a magnet. This would involve a large aperature magnet (e.g., an ANL type BM 109 with a 8" x 24" x 72" aperature and maximum integral Bdl of 1366 KG-in) placed immediately downstream of the second spark chamber module followed by a third spark chamber module 5 meters from the magnet. All tracks with lab momentum $\gtrsim$ 100 GeV/c and with transverse momentum $\lesssim$ 1 GeV/c will be transmitted through the aperature of the magnet and will be recorded in the third spark chamber module. The deflection in the magnet, coupled with the long lever arm, provides a $\pm\Delta p/p \approx .012$ p (%). Thus, 6-7% $\pm\Delta p/p$ or less can be achieved for all tracks of interest without altering the initial setup of the experiment.

(B) Spark Chamber Optics

The wide gap chambers have an active volume 8" deep x 48" high x 36" wide per cell. Each chamber consists of 2 cells and each module consists of 2 chambers, as seen in Figure 7. The chambers are mounted on a precision platform which has three primary functions: 1) Providing a means of determining the relative locations of the two chamber modules and the bubble chamber, 2) Providing a means of maintaining a continuous check on these positions and 3) Providing a simple means of re-installing the apparatus in the beam line after removal. Measuring of apparatus locations is done by means of two theodolites, one to determine and monitor bubble chamber-spark chamber platform positions and the second to determine and monitor spark chamber-spark chamber platform positions. Leveling legs on the chambers, top, bottom, front, and rear fiducials on the chamber frame and fiducials on the precision platform serve to position the chambers in a known orientation. Front and top fiducials also appear on each film frame to orient the chambers on the film. Rear and bottom fiducials on periodically run fiducial runs serve to complete a three dimensional co-ordinate system for track reconstruction independent of knowledge of camera position. Additional platform fiducials in view of the camera can serve as an extra check on spark chamber-platform orientations.

The chamber separation is variable within and between modules. Within the module a maximum separation of 32" is allowed. As seen in Figure 8, this maximum separation still permits viewing both chambers in a module with one 35 mm. camera at a demagnification of 64:1. This demagnification is an upper limit permitted by the intrinsic resolution of a film such as Kodak Shellburst for a real space position accuracy of 0.1 mm. With a 4" lens

the camera can be located at 20 ft. from the center of the chambers. The chambers are inclined 6° relative to the beam line to permit a direct view in each chamber, thereby eliminating lenses and mirrors in that view (see Figure 9). The chamber windows are made of 10 mil. clear Mylar to eliminate distortions there. One precision mirror is used in the 90° stereo view to bring that view to the same camera. A fiducial plane with many fiducials is located at the bottom of the spark chamber to permit corrections due to any distortions in the mirror. 90° stereo is used for maximum accuracy in reconstruction. The direct view is the view of the plane of bend for maximum accuracy in momentum determination. A strip mirror subtending $\sim$ 1/3 of the gap in the direct view provides 10° stereo for resolving ambiguities in track reconstruction. The mirror subtends only part of one gap in each chamber to eliminate confusion between the direct and 10° stereo tracks. A dark room under slight over pressure surrounds each assembly for photographic and hydrogen safety reasons.

(C) Gamma-Ray Detection

The insertion of several radiation lengths of material between the second and third gaps of the spark chamber units will provide an effective converter for gamma-rays from fast, forward π°'s. From the point of interaction, probably measureable to $\lesssim$ 5 mm, both the frequency and direction of fast π°'s can be inferred. To our knowledge, the only previous measurement of π° frequency is that of Elbert et al.[6] at 25 GeV/c for $\pi^{-}p$ in a hydrogen bubble chamber with plates. Their results, although somewhat weak statistically, are in rather strong disagreement with the multiperipheral model. Clearly, more precise measurements at NAL energies will be very valuable in our proposed studies.

(D) Trigger Schemes

The trigger arrangement will be designed such that the spark chambers fire on virtually all interactions, there being nearly one per beam burst. A picture of the bubble chamber will be taken for each expansion. Two simple and flexible schemes have been devised:

(1) Energy-Loss Trigger: Referring to Figure 1, multiparticle-charge-particle secondaries would be selected by pulse-height criteria in the counters S_3 S_4 S_5. More than one particle will, on the average, give a greater pulse height than that for a single beam particle. Although one might consider almost any type of counter which gives signals proportional to the number of particles which transverse it, e.g. Cerenkov, scintillation, etc., the most simple to utilize is the scintillation counter and it also turns out to result in the thinnest detector (in g/cm^2). A single scintillation counter when traversed by a high energy particle will give a Landau pulse-height distribution. This distribution, with its long tail at high pulse heights, cannot be avoided in the present application. A pulse height of 2 times the minimum value will occur on traversal by a single minimum ionizing particle $\sim$5% of the time. This can be greatly improved, however, if two or more counters S_1, S_2; S_3 $S_4 \ldots S_n$ are utilized and the minimum pulse height appearing is considered. In this case, the width of the distribution will be decreased by $1/\sqrt{n}$ and even for n = 3, the tail has all but vanished. If this signal is to be used to trigger the downstream chambers, the minimum pulse height must be determined in $<<1$ μ sec.

With this method, it is to be noted that the downstream counters should be thin in order that nuclear interactions in them do not occur frequently. Such interactions are no different in character from those in the chamber and

walls and triggers due to them would certainly result. The number of these should be much smaller than those which occur in the chamber. In 1 mm of plastic scintillator a minimum ionizing particle produces $\sim 10^3$ photons. With an efficient photo cathode ($\sim$25%) and a light collection efficiency of $\sim$20%, 50 photo-electrons could result. This number is sufficient to assure that statistical fluxtuations will be relatively small. The five counters, S_1, S_2, S_3, S_4, and S_5, would represent a total thickness of 0.5 cm which is 0.5cm/52cm = 1/100 of a geometrical-mean-free-path. Thus, with 6 particles per picture and with the counters described, in $\sim$ 6% of the pulses would the spark chamber system have recorded interactions occuring in the triggering counters $S_1S_2S_3S_4$and S_5.

For reasons of efficient and uniform light collection the size of these counters probably should not exceed 8" x 8". This presents some minor limitations in the detection of secondaries as they must appear within a cone of $\pm 3°$ if placed at a distance of $\sim$2 meters from the interaction. It may be possible to locate counters nearer the chamber inside the iron yoke, and if so the acceptance angle would be increased. This setup is very inefficient for elastic scattering and processes of the type $pp \rightarrow ppn(\pi°)$, when the struck proton is slow and at a large angle, thus missing $S_3S_4S_5$. However, an alternate scheme, discussed next, would resolve this shortcoming. Also, with this arrangment one also might consider triggering on events with no charged secondary within the angular acceptance of $S_3S_4$and S_5. This alternate trigger could be tried with parallel logic and could be easily included or not as a parallel trigger.

(2) Beam-Deflection Trigger: The trigger consists of a 3.0 inch diameter scintillator S_3 located in the beam 125 feet downstream from the

bubble chamber (see Figure 1). When this scintillator fails to record a particle previously observed by counters S_1, S_2 in the beam upstream of the bubble chamber, it is considered to have interacted.

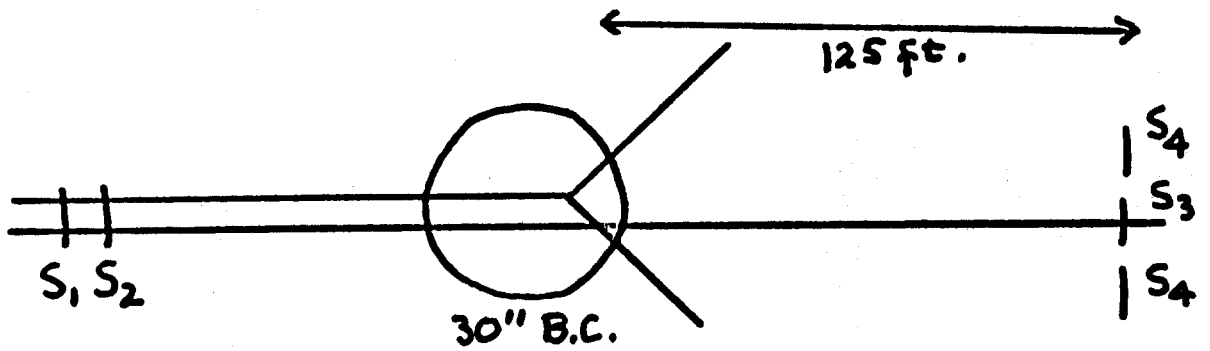

For the purposes of investigating the properties of the trigger we assume a 2.0" diameter beam in the bubble chamber. This allows a beam spread which does not diverge after leaving the chamber except for multiple Coulomb scattering. For beam momenta between 100 and 500 GeV/c the beam size at the downstream scintillator should not exceed 2.25 inches due to multiple scattering.

This trigger fails most frequently in detecting elastic scatters. Table II below lists the average minimum scatter angle and recoil range for elastic events which will actuate the trigger.

TABLE II - Minimum Angle and Recoil Range For Elastic Events

Beam Momentum GeV/c	Minimum Scatter Angle mr.	Minimum Recoil Range cm
100	1	0.3
200	1	3.5
300	1	15.0
500	1	100

There is considerable flexibility here. For example, by moving S_3 to 200 feet downstream of the bubble chamber and using a diameter of 2.5"

instead of 3.0", one achieves a minimum angle of 0.5 mr. and a minimum range of 8.0 cm at 500 GeV/c.

Some fraction of the inelastic events might also be expected to put a particle through S_3, invalidating the trigger. Scaling 25 GeV/c events to NAL energies indicates this is not very important, in part because the bubble chamber field imparts transverse momentum to a track which is several times that of the minimum detectable elastic scatter. For example at 200 GeV/c this trigger fails on 4.5% of the 2-prongs, 3% of the 4-prongs, 1% of the 6-prongs and 0.3% of the 8-prongs.

This small loss of inelastic events can be reduced somewhat by surrounding S_3 with a larger counter S_4. A hole in S_4 passes beam particles on to S_3. A multiparticle accidental through S_3 is likely to be accompanied by one or more particles through S_4. Hence one would trigger on $(S_1.S_2.\overline{S_3}.S_4)$, $(S_1.S_2.\overline{S_3}.\overline{S_4})$, $(S_1.S_2.S_3.S_4)$. One can reduce the loss rate arbitrarily by increasing the size of S_4 or moving it closer to the bubble chamber.

S_3 was not placed more than 125 feet downstream of the bubble chamber so that transit time of the particles and signals would be short enough to allow adequate time to perform logical operations and apply spark chamber voltages in less than 500 ns. This restriction is probably too strict by at least a factor of two and can probably be relaxed to observe smaller angle elastic scatters. Some groups will probably prefer a beam profile in the chamber more like 5" x 1/2". In this case S_3 would be about 6.5" x 1". This has approximately the same solid angle as the circular counter discussed above and presents no focusing problems for the presently planned beam.

Finally, it is emphasized that both these triggers are flexible and most certainly can be studied quickly and efficiently under test beam condi-

tions. It would be our intention to do so before proceeding with "production" data-taking.

REFERENCES (Sections I and II)

1. R. Hagedorn, Suppl. Nuovo Cimento 3, 147 (1965)
   R. Hagedorn and J. Ranft, Suppl. Nuovo Cimento 6, 169 (1968)
   R. Hagedorn, Suppl. Nuovo Cimento 6, 311 (1968)
2. H. Grote, R. Hagedorn and J. Ranft, "Atlas of Particle Production Spectra", CERN 1970
3. J. Lach and S. Pruss, "Hadron Beams in the Neutrino Area", TM-285
4. R. P. Feynman, p.237, "High Energy Collisions", Stony Brook (Gordon and Breach, 1969)
   R. P. Feynamn, Phys. Rev. Letters 23, 1415 (1969)
5. J. Benecke, T. T. Chou, C. N. Yang , E. Yen, Phys. Rev. 188, 2159 (1970)
6. Bali, Brown, Peccei and Pignòtti, Phys. Reb. Letters 25, 557 (1970)
7. C. P. Wang, Phys. Rev. 180, 1463 (1969); Nuovo Cimento 64A, 546 (1969); Physics Letters 30B, 115 (1969)
8. J. Ranft, Physics Letters 31B, 529 (1970)
9. J. C. Vander Velde, Physics Letters 32B, 501 (1970)
10. R. W. Anthony et al., Phys. Rev. Letters 26, 38 (1971)
11. Chan, Wang, Wong, Phys. Rev. Letters 26, 280 (1971)
12. R. Hagedorn, Nuclear Physics B24, 93 (1970)
13. W. Walker, p.295, "High Energy Collisions", Stony Brook (Gordon and Breach, 1969)
14. L. Bertochi and E. Ferrari, p.71, Volume II, "High Energy Physics", (Academic Press, 1967)
15. D. H. Miller, NAL SS69, Volume 2, p.35
16. A. Erwin, Conference on Expectations for Particle Reactions at the New Accelerator (Wisconsin, March 1970)
17. P. Söding, Physics Letters 8, 285 (1964)
18. N. N. Khuri and T. Kinoshita, Phys. Rev. 137, B720 (1965); Phys. Rev. 140, B707 (1965); Phys. Rev. Letters 14, 84 (1965)
19. R. Armenteros and B. French, p.237, Volume IV, "High Energy Physics" (Academic Press, 1969)

REFERENCES (SECTION IV)

1. T. H. Fields, et al., NAL Summer Study, Vol. 3, 227 (1968).
2. "Hadron Beams in the neutrino Area", J. Lach and S. Pruss, NAL Report TM-285, 2254.000.
3. "Extrapolated Ratios of K^- and $\bar{p}$ to π^- from High Energy Protons on Aluminum measured at Serpukhov," V. E. Barnes, Purdue University High Energy Physics Note # 313, April 1, 1971.
4. S. Pruss, NAL Summer Study (1970) p. 103.
5. M. Atac and J. Lach, Nucl. Instr. & Methods 86, (1970) p. 173.
6. J. W. Elbert et al., Nuclear Physics B19, 85 (1970).

Figure Caption (Section I)

Fig. 1: π^- yields at the target versus particle ratios $\frac{K^-}{\pi^-}$ and $\frac{\bar{p}}{\pi^-}$ at the bubble chamber (1000 m away from the target) for pp collisions at 500 GeV. The results are obtained from the Hagedorn-Ranft model[1,2]. The solid curves represent lines of constant secondary momentum, starting at 150 GeV and increasing in steps of 50 GeV, and the dashed curves are production angles starting at 0 degree and increasing in steps of .1 degree. The proposed point of operation is indicated by the two circles in the figure.

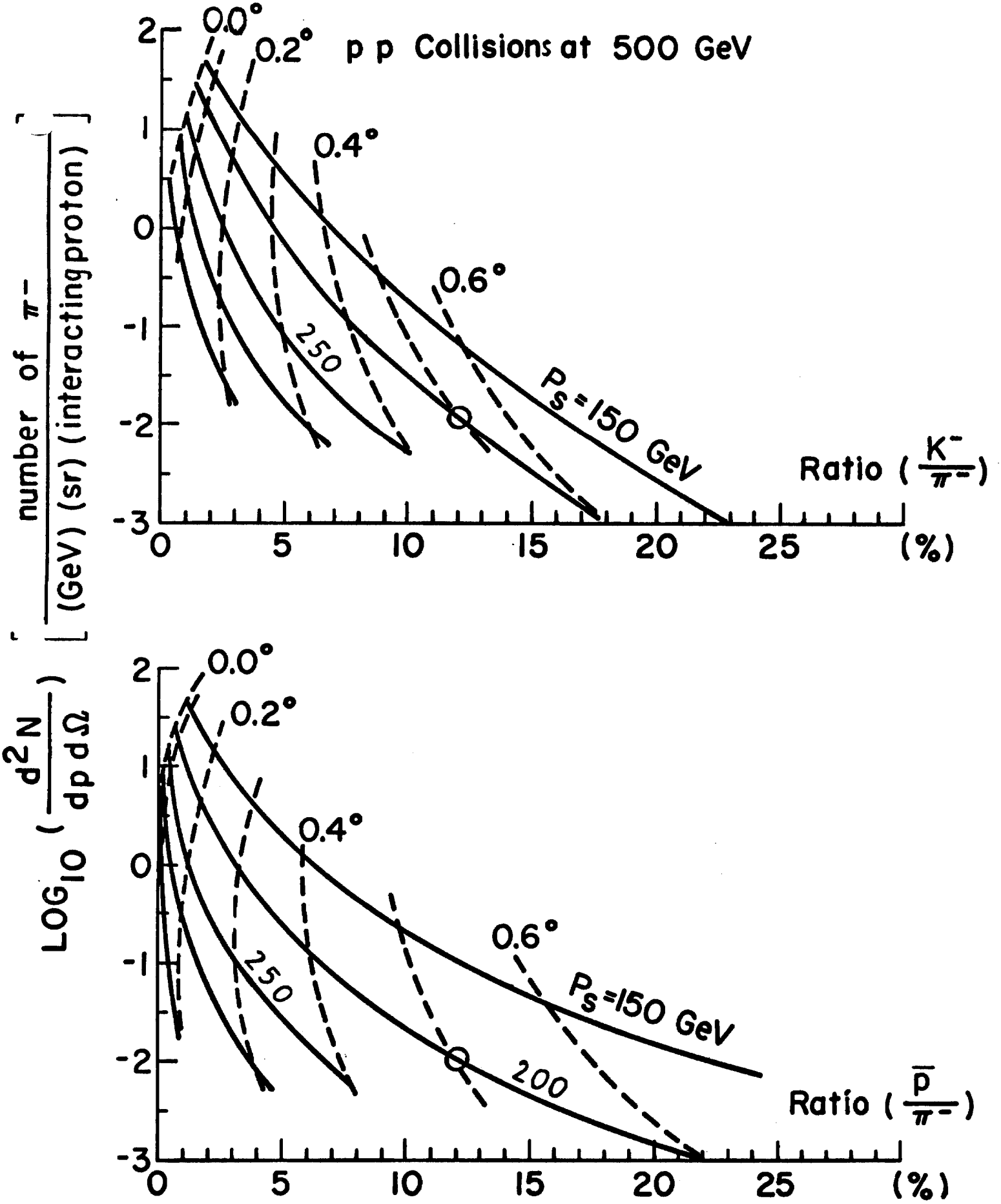

Fig. 1 (Section I)

FIGURE CAPTIONS (Section IV)

Fig. 1 Components of the proposed hybrid system.

Fig. 2 Contours of laboratory angle and momentum on the Peyrou Plot for the π in the reaction $p + p \rightarrow \pi^+ + \ldots$ at 500 GeV/c.

Fig. 3 Shows more detail of Fig. 2.

Fig. 4 Detail of contours of laboratory angle and momentum on the Peyrou Plot for the proton in the reaction $p + p \rightarrow p + \ldots$ at 200 GeV/c.

Fig. 5 Upstream proportional wire spectrometer.

Fig. 6 Calculated momentum resolution for the apparatus of Fig. 1.

Fig. 7 Wide gap optical spark chamber (one of two such chambers).

Fig. 8 Wide gap optical spark chambers and camera positioning.

Fig. 9 Format of images on 35 mm film.

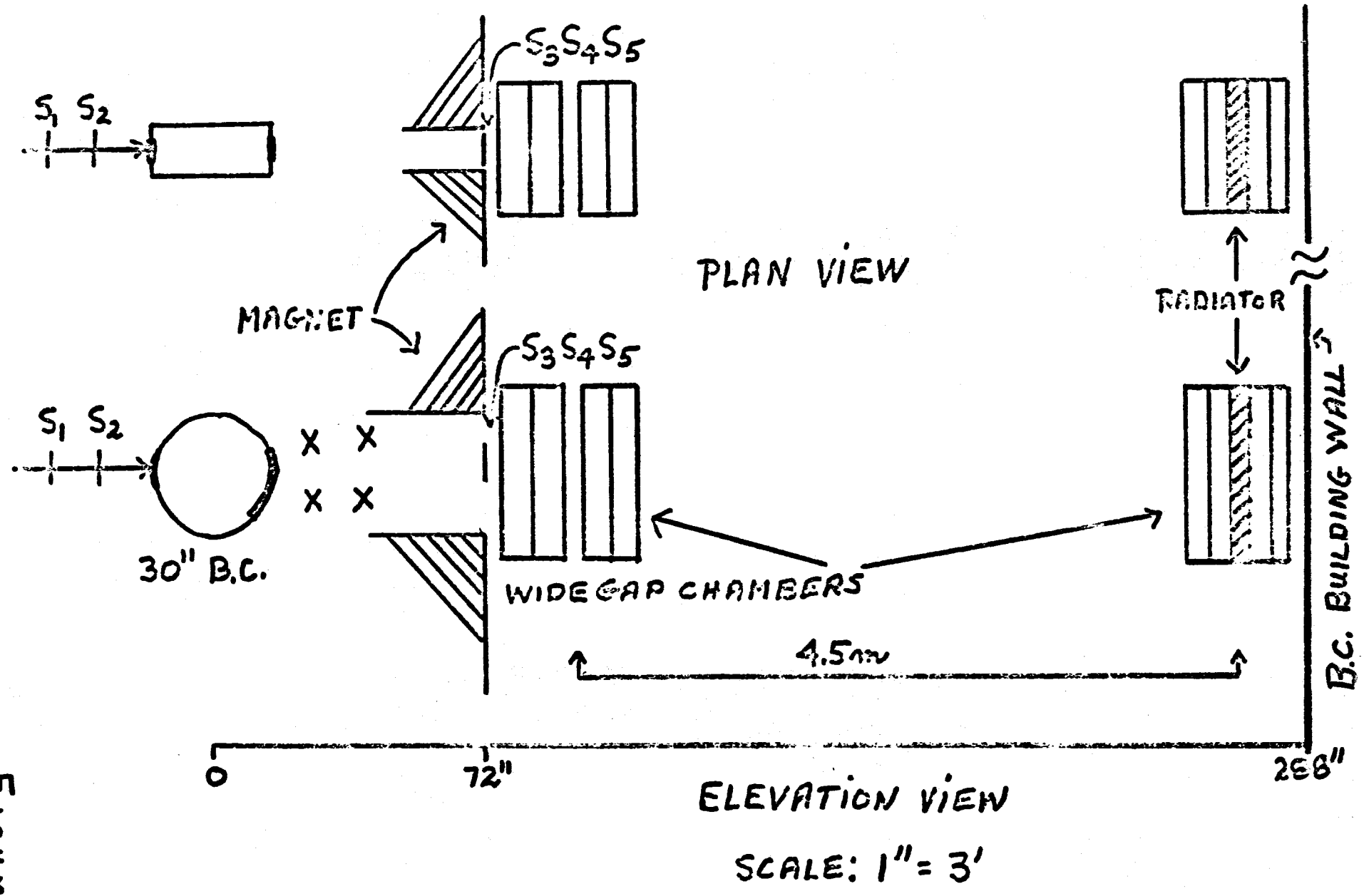
S1 S2
S3 S4 S5
MAGNET
PLAN VIEW
RADIATOR
B.C. BUILDING WALL
30" B.C.
WIDE GAP CHAMBERS
4.5m
0
72"
288"
ELEVATION VIEW
SCALE: 1" = 3'

Figure 1

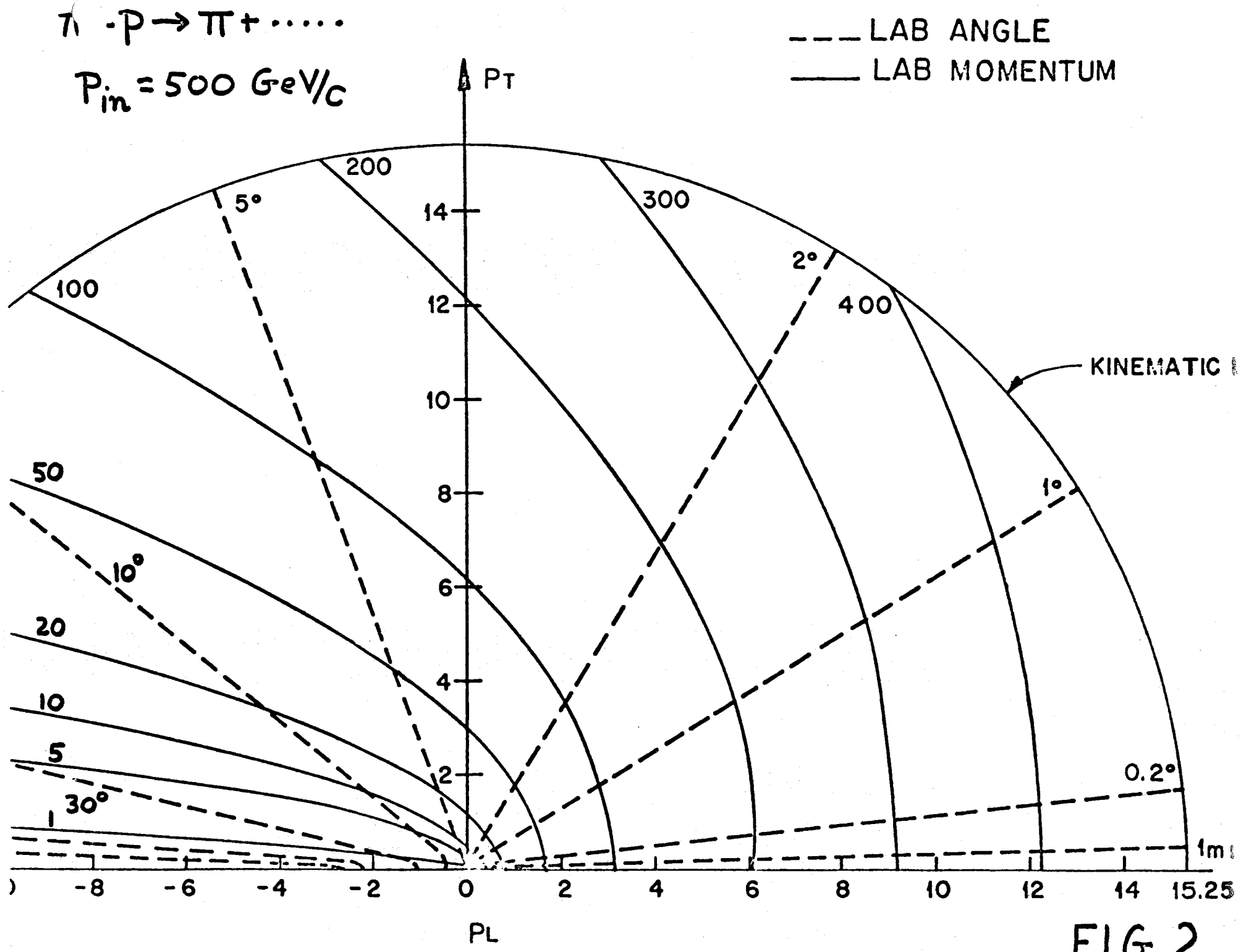
π - P → π + · · · · ·
P_in = 500 GeV/c
LAB ANGLE
LAB MOMENTUM
PT
PL
KINEMATIC
100
200
300
400
50
20
10
5
1
5°
2°
1°
0.2°
1m
10°
30°
14
12
10
8
6
4
2
-8
-6
-4
-2
0
2
4
6
8
10
12
14
15.25

FIG. 2

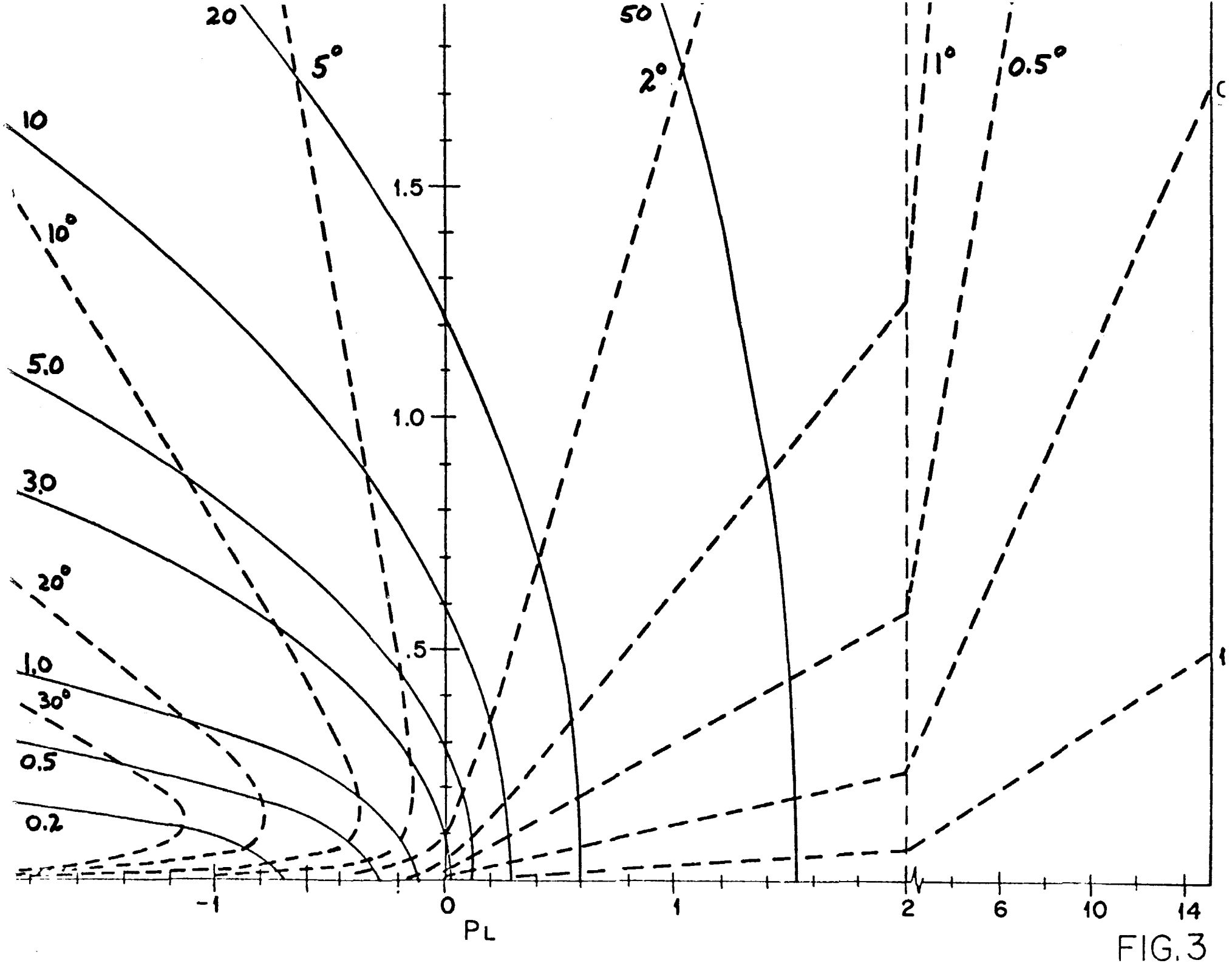

FIG. 3

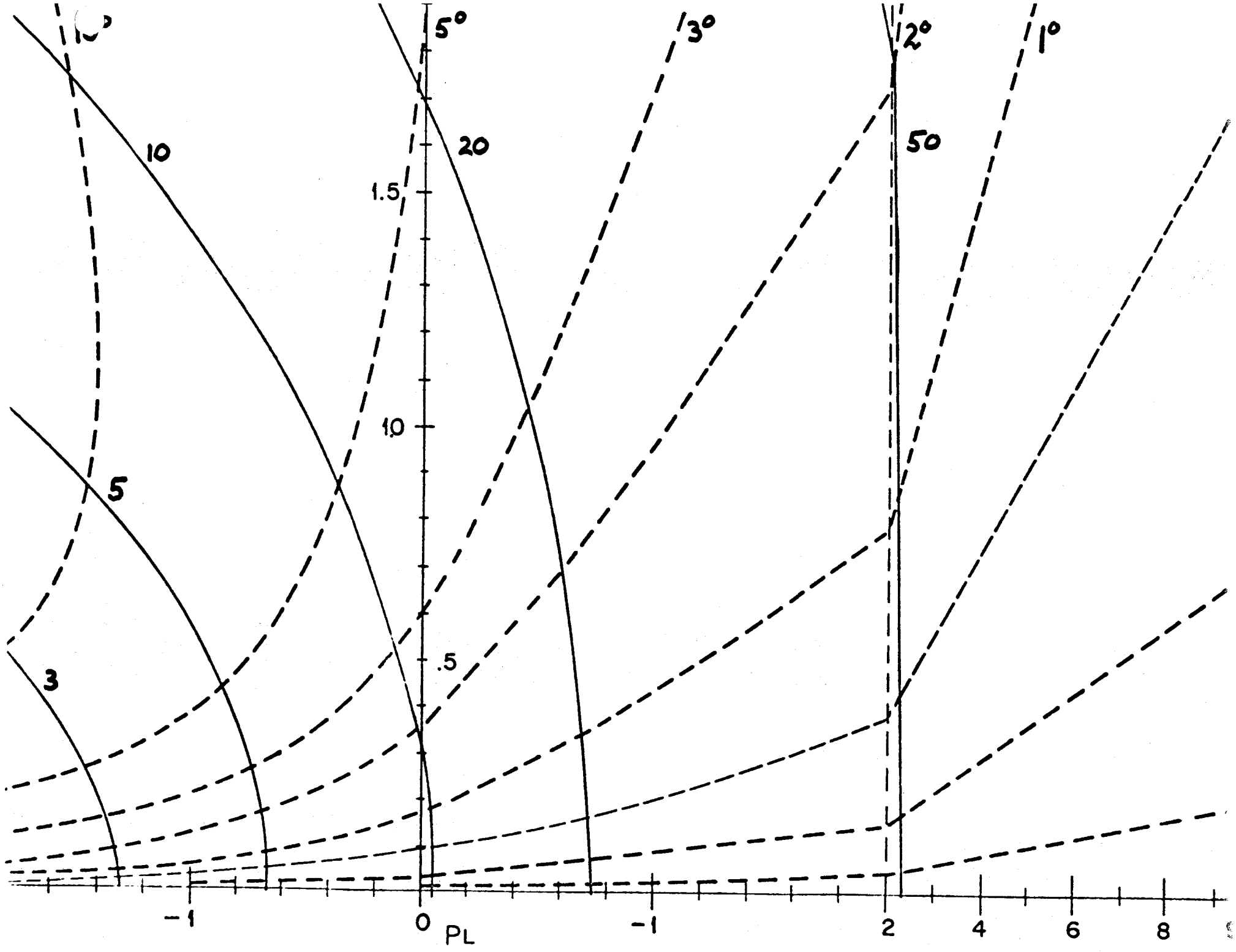

FIG.4

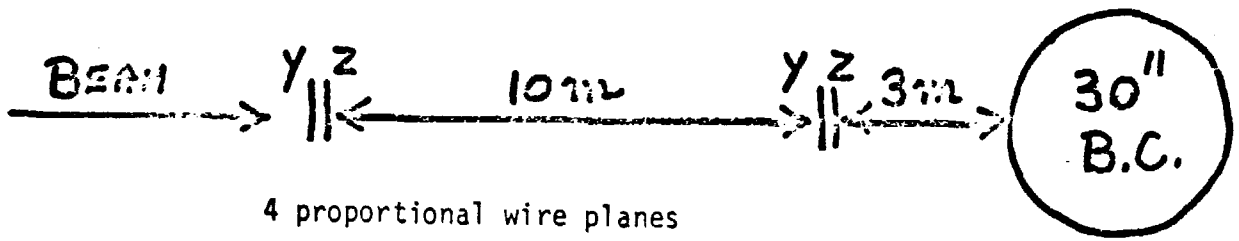

4 proportional wire planes

1 mm wire spacing

2"x2", 50 wires. This can be scaled up by a factor 2 in y if needed.

The momentum defining proportional chamber is not shown, being over 1000' upstream at a focus where the image of the target is ∿2 mm in size. The dispersion is ∿2 "/% at this point.

FIGURE 5

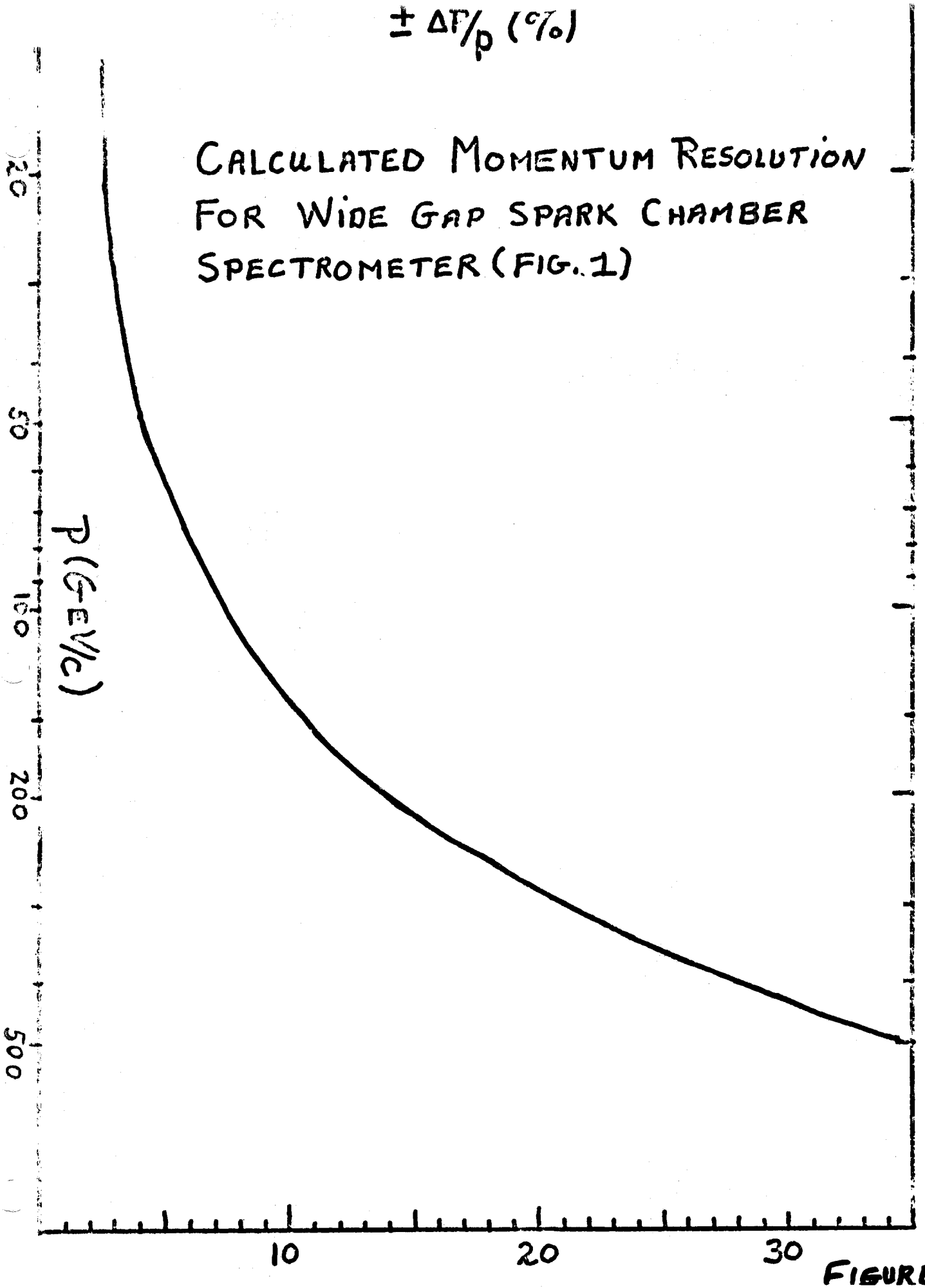
± ΔP/p (%)
CALCULATED MOMENTUM RESOLUTION FOR WIDE GAP SPARK CHAMBER SPECTROMETER (FIG. 1)
P (GeV/c)
20
50
100
200
500
10
20
30

FIGURE 6

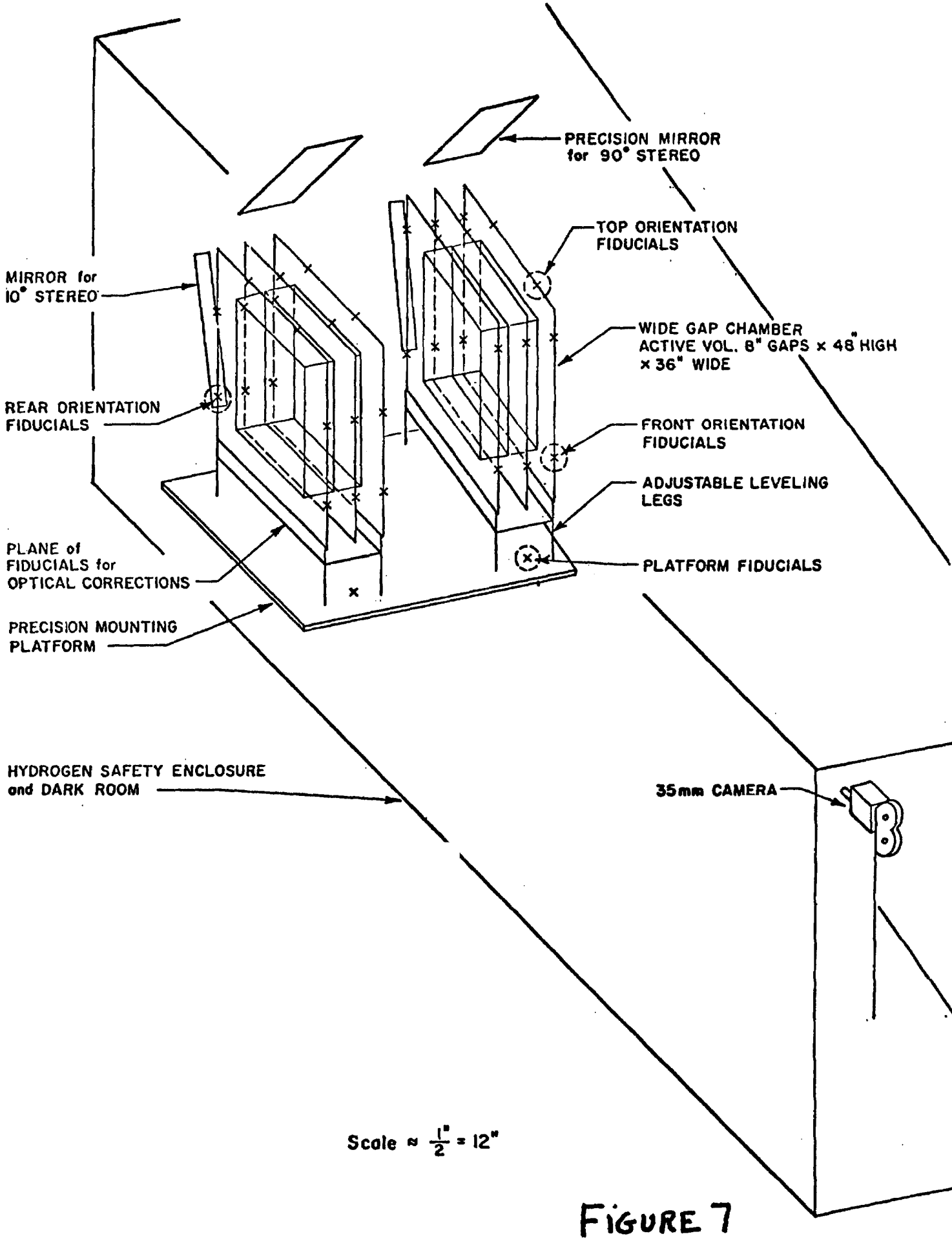
PRECISION MIRROR for 90° STEREO
TOP ORIENTATION FIDUCIALS
MIRROR for 10° STEREO
WIDE GAP CHAMBER ACTIVE VOL. 8" GAPS x 48" HIGH x 36" WIDE
REAR ORIENTATION FIDUCIALS
FRONT ORIENTATION FIDUCIALS
ADJUSTABLE LEVELING LEGS
PLANE of FIDUCIALS for OPTICAL CORRECTIONS
PLATFORM FIDUCIALS
PRECISION MOUNTING PLATFORM
HYDROGEN SAFETY ENCLOSURE and DARK ROOM
35mm CAMERA
Scale ≈ 1"/2 = 12"

FIGURE 7

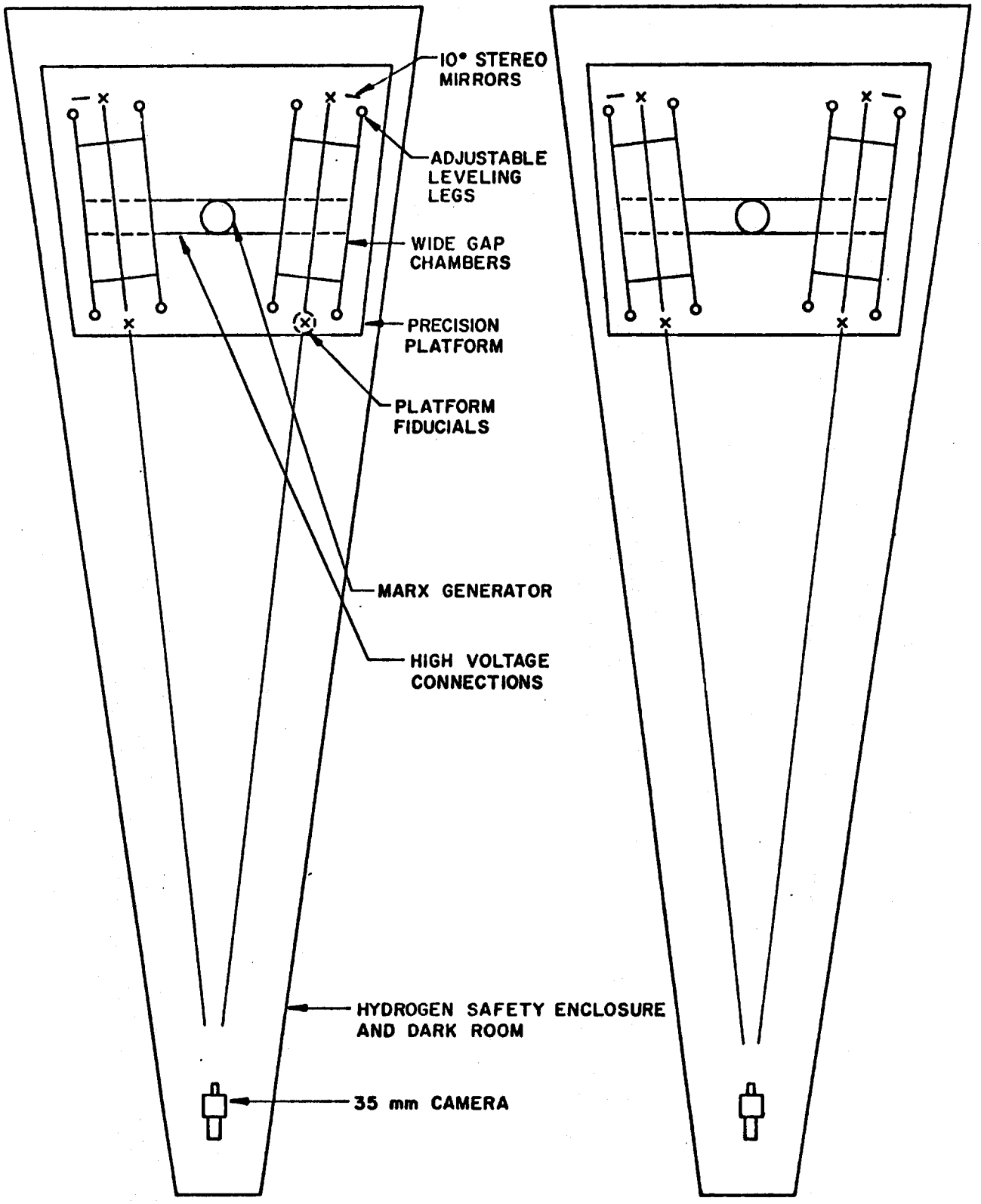

PLAN VIEW
SCALE ≈ $\frac{1}{2}$" = 12"

FIGURE 8

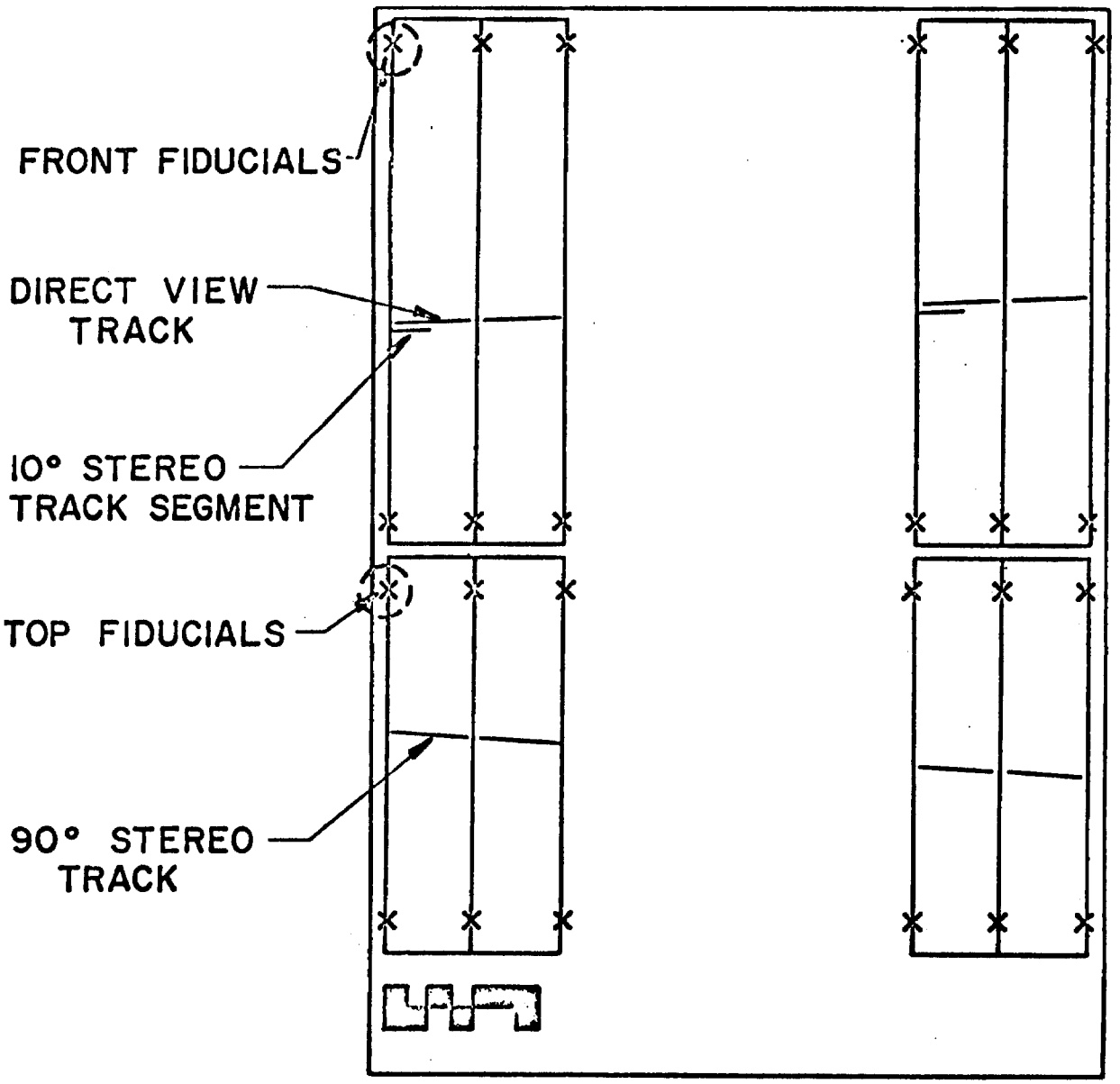

FILM FORMAT 35 mm 1.5" × 1.0"

FIGURE 9

SUBJECT: K^- and $\bar{p}$ Fluxes in the 1000 Meter Hadron Beam and Event Rates in the 30" Bubble Chamber.

NAME Virgil E. Barnes

DATE April 21, 1971

APPENDIX I.

Serpukhov data published in Physics Letters indicate that $\bar{p}$ and K^- as a fraction of π^- are increasing with bombarding energy,[1] at a fixed value of p_-/p_{max} where p_- is the outgoing K^- or $\bar{p}$ laboratory momentum and p_{max} is roughly the bombarding momentum. Also, these fractions increase as p_-/p_{max} becomes smaller. More recent Serpukhov data[2] at 70 GeV, which go to lower values of p_-/p_{max}, show that the richest ratios occur for $p_-/p_{max} = 0.2$. The table on the following page is for $p_-/p_{max} = 0.2$ and 0.4. Due to substantial K^- decay over the 1000 meter beam length, the ratio $R(K^-)$ is roughly a constant 5% over this range of p/p_{max}, when the bombarding energy is 500 GeV.

For out choice of a 130 GeV secondary beam ($p/p_{max} = 0.26$) using the methods outlined on the next page we have at the bubble chamber:

$P_{primary\ proton}$	500 GeV	200 GeV
K^-/π^-	4.7%	1.4%
$\bar{p}/\pi^-$	6.7%	0.4%

We base our event rates on a 15" fiducial volume, 10 Hadron tracks per picture, and a 200,000 picture exposure, giving 2.74 events/μb. We estimate $\sigma(\pi^- p) = 24.5$ mb, $\sigma(K^- p) = 21$ mb, and $\sigma(\bar{p}p) = 42$ mb above 100 GeV, equal to the measured Serpukhov cross sections at around 60 GeV.

130 GeV/c Interactions	$P_{proton} = 500$ GeV/c	$P_{proton} = 200$ GeV/c
$\pi^- p$	61,000 events	67,000 events
$K^- p$	2,400	800
$\bar{p}\ p$	6,800	460

We expect K^- and $\bar{p}$ to be negligible when the momentum is near p_{max}.

REFERENCES

1. F. Binon et al., Phys. Lett. 30B, 506 (1969).
2. Yu M. Antipov et al., Phys. Lett. 34B, 164 (1971)

APPENDIX

Extrapolated Ratios of K^- and $\bar{p}$ to π^-, from High Energy Protons on Aluminum, measured at Serpukhov.

Figure 1 suggests that $R(K^-)$ and $R(\bar{p})$, defined as fractions of outgoing π^-, increase with proton bombarding energy from 19 to 78 GeV for a fixed value of P_{K^-}/P_{max} or $P_{\bar{p}}/P_{max}$.

Figure 2 shows this variation, for $P^-/P_{max} = 0.4$. Both R's seem to increase logarithmically with $P_{inc.}$, and have been so extrapolated. Similar trends obtain for $P^-/P_{max} = 0.5$ and 0.6.

Figure 3 extends the "universal" shape of Figure 1 down to $P^-/P_{max} = 0.1$ and shows that the R's peak when $P^-/P_{max} \sim 0.2$. $R(K^-)$ increases by a factor ~1.8 and $R(\bar{p})$ increases by a factor ~5 when P^-/P_{max} goes from 0.4 to 0.2 (at $P_{inc.} = 70$ Gev/c).

We thus estimate the following ratios. Decays of π^- and K^- over a 1,000 meter beam length are taken from Table I. $R(K^-)$ suffers; but $R(\bar{p})$ improves from decay of π^-.

500 GeV p on Al.		% of π^-	1000m, % of π^-	200 GeV p on Al		% of π^-	1000m, % of π^-
100 GeV	K^-	18%	5.6%	40 GeV	K^-	14%	0.77%
200 GeV	K^-	8%	4.5%	80 GeV	K^-	8%	1.85%
100 GeV	$\bar{p}$	13%	15.5%	40 GeV	$\bar{p}$	10%	15.60%
200 GeV	$\bar{p}$	2%	2.2%	80 GeV	$\bar{p}$	2%	2.50%

Hagedorn-Ranft calculations also indicate ratios about like this at production angles of 5 to 10 mrad, while at 0° production the Hagedorn-Ranft ratios are considerably smaller, as in the figures of the NAL report on Hadron Beams to the Bubble Chambers, by J. Lach and S. Pruss, TM-285

2254.000

APPENDIX I

TABLE I

1000 Meter Beam, K^- and π^- Decays

P- (GeV/c)	30	40	50	80	100	120	150	200	300	400	500
K^-, % Remaining	1.1	3.5	7.3	18.5	26	32	41	51	64	72	77
π^-, % Remaining	55	64	70	80	84	90	91	91.5	94	95.5	97.5
R_D decay ratio K^-/π^-	0.02	0.055	0.104	0.23	0.31	0.36	0.45	0.56	0.68	0.76	0.79

$\beta\gamma = P/m$	$c\tau_{K^-} = 3.7$ m	$\beta\gamma c\tau = p(\text{GeV}) \times 7.4$	$N/N_o = e^{-L/7.4p} = e^{\frac{-135}{p}}$
$N = N_o\, e^{-(L/\beta\gamma c\tau)}$			
$L = 1000$ m	$c\tau_{\pi^-} = 7.81$ m	$\beta\gamma c\tau = p(\text{GeV}) \times 55.8$	$N/N_o = e^{-L/55.8P} = e^{\frac{-18}{P}}$

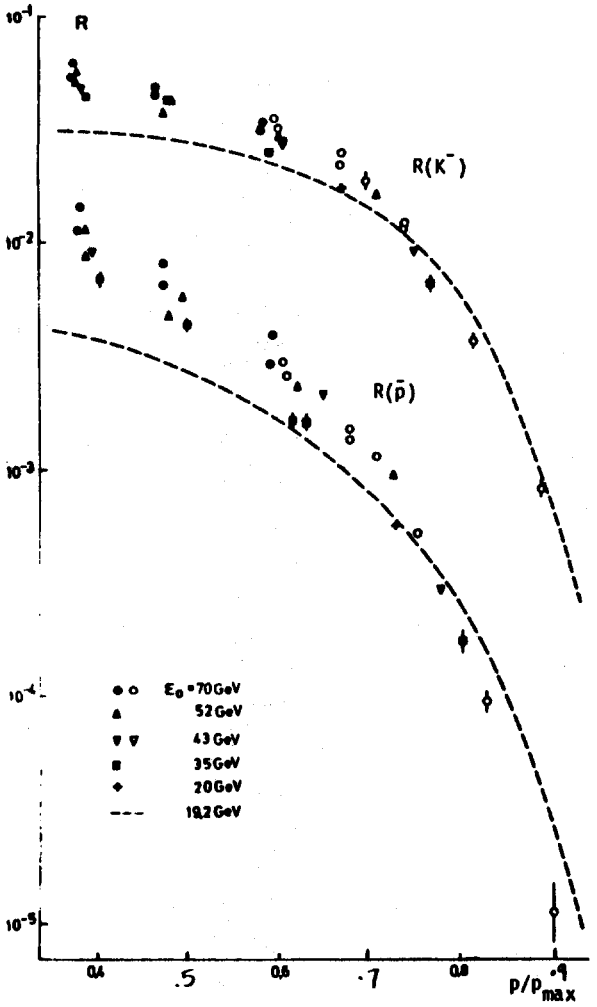

Fig. 3. Production ratios R as a function of p/p_{max}. The broken curves refer to p-p collisions [4] at 19.2 GeV.

is observed for the ratio $R(K^-)$ but it is somewhat less pronounced.

The differential cross-sections for the production of particles were obtained by a method already described [1]. The computed beam luminosity $\Delta\Omega \cdot \Delta p$ was used for their evaluation. The computed value of Δp, the momentum acceptance, has been checked in a measurement made with the differential Čerenkov counter. The relative flux of protons hitting the aluminium target was deduced from the measurement of the induced ^{22}Na activity. Absolute values of the cross-sections have been obtained by normalizing the data with the 40 GeV/c value [1].

The differential cross-sections for π^- production in aluminium by 70 GeV/c protons are given in table 1. The flux of π^- keeps increasing quickly as momentum decreases down to 25 GeV/c. It is multiplied by a factor of 3 by going from 40 GeV/c to 25 GeV/c.

In the region of low momentum at the IHEP synchrotron, it should be possible to obtain intense beams of antiprotons. Already, at a momentum of 25 GeV/c, for a 1 GeV/c momentum bite, the flux of antiprotons is larger than 10^4 per burst.

References

1. Yu. B. Bushnin, S. P. Denisov, S. V. Donskov, A. F. Dunaitsev, Yu. P. Gorin, V. A. Kachanov, Yu. S. Khodirev, V. I. Kotov, V. M. Kutyin, A. I. Petrukhin, Yu. D. Prokoshkin, E. A. Razuvaev, R. S. Shuvalov and D. A. Stoyanova, J. V. Allaby, F. Binon, A. N. Diddens, P. Duteil, G. Giacomelli, R. Meunier, J.-P. Peigneux, K. Schlupmann, M. Spighel, C. A. Ståhlbrandt, J.-P. Stroot and A. M. Wetherell, Preprint IHEP 69-18 (1969), Phys. Letters 29B (1969) 48.
2. F. Binon, S. P. Denisov, P. Duteil, V. A. Kachanov, V. M. Kutyin, Yu. D. Prokoshkin, E. A. Razuvaev, R. S. Shuvalov, M. Spighel and J.-P. Stroot, Int. Conf. on Elementary particles, Lund, 1969.
3. J. V. Allaby, Yu. B. Bushnin, S. P. Denisov, A. N. Diddens, R. W. Dobinson, S. V. Donskov, G. Giacomelli, Yu. P. Gorin, A. Klovning, A. I. Petrukhin, Yu. D. Prokoshkin, R. S. Shuvalov, C. A. Ståhlbrandt and D. A. Stoyanova, Int. Conf. on Elementary particles, Lund, 1969, Phys. Letters 30B (1969) 500.
4. J. V. Allaby, F. Binon, A. N. Diddens, P. Duteil, A. Klovning, R. Meunier, J.-P. Peigneux, E. L. Sacharidis, K. Schlupmann, M. Spighel, J.-P. Stroot, A. M. Thorndike and A. M. Wetherell, Paper submitted to the 14th Int. Conf. on High-energy physics, Vienna (1968) (CERN, Geneva, 1968).

* * * * *

FIGURE 1

Appendix I

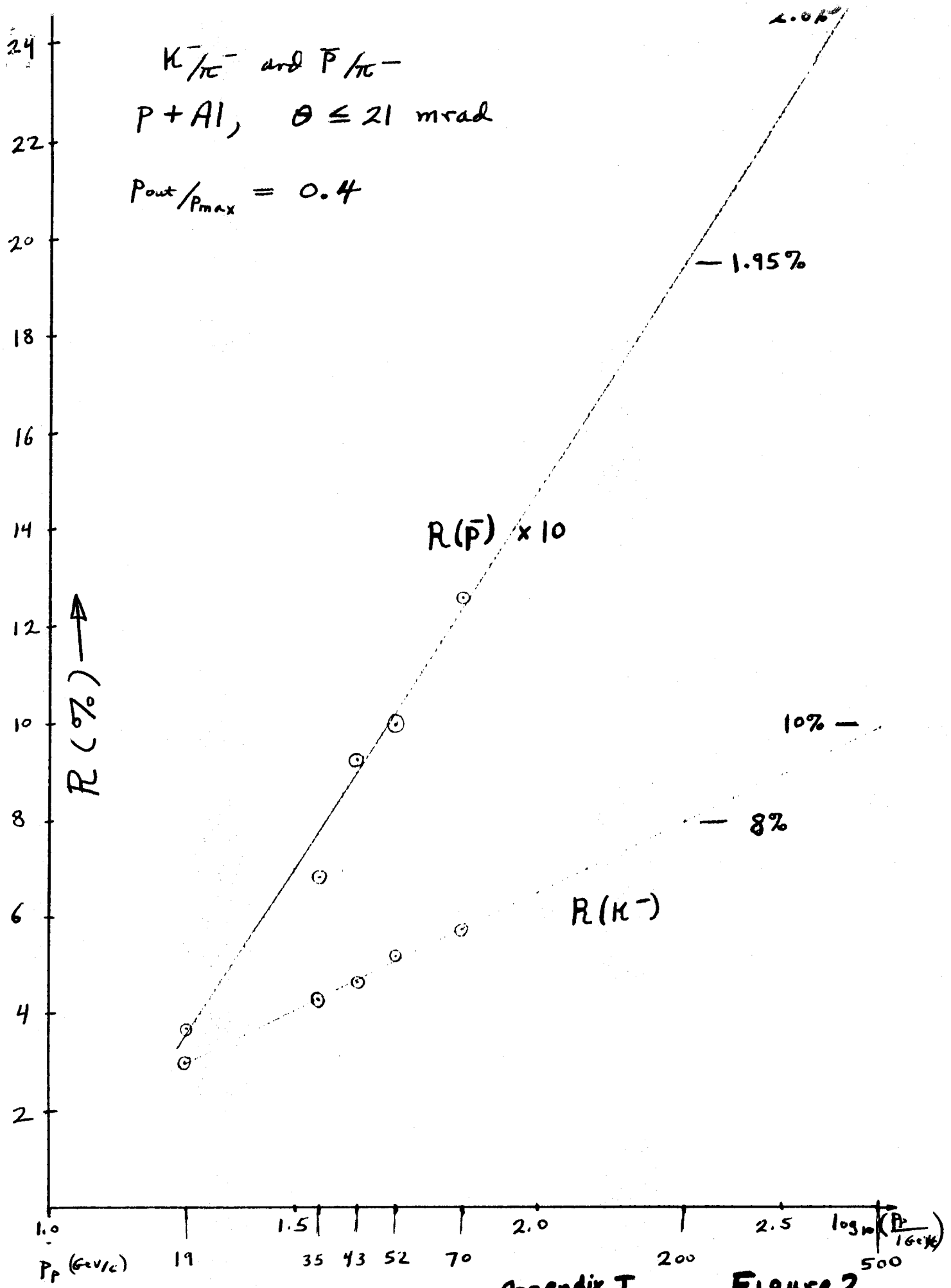

Appendix I, Figure 2

$(d^2\sigma_{K^-}/d\Omega dP)/(d^2\sigma_{\pi^-}/d\Omega dP)$ and analogous values for antiprotons ($R_{\bar{p}}$) and antideuterons ($P_{\bar{d}}$) are presented in table 1. Corrections, that take into account particle decay and their interaction with the matter in the beam path, were introduced into the measured values. Due to a very big length of the beam channel (≈ 120 m) the correction for kaon decay was $\approx 400\%$. In order to check whether this correction had been defined properly, the relative ammount of kaons in the beam was measured at two points at the end and in the middle of the beam, at a ≈ 80 m distance from the target. The values obtained for R_{K^-} coincided with an accuracy of 3% for $P = 10$ GeV/c and of 2% for $P = 13.3$ GeV/c.

As becomes obvious from table 1, the relative yield of heavy particles R from the Al target is somewhat heigher than from the Be target, however this difference is not very great. In the present paper the measurements were made at angles θ different from 0. As it was noted earlier [2-3] the relative yields R depend weakly on θ. So, at $P = 39$ GeV/c the ratio $R_{\bar{p}}$ increases by $(35 \pm 4)\%$ with the increase of the square transferred momentum $t \approx p^2\theta^2$ from 0 to 0.7 (GeV/c)^2. If we approximate this dependence with the experimental $R_{\bar{p}}(t) \approx \exp(-at)$, and assume that it is valid in the region of small momenta P, then the difference between the relative antiproton yields at $\theta = 0$ and 47 mrad and $P = 13.3$ GeV/c will be 15%, and for $P = 10$ GeV/c and $\theta = 0$, $R_{\bar{p}}$ practically coincides with the value, measured at $\theta = 27$ mrad.

The measured values R are presented in fig. 1 together with the data, obtained at larger momenta [2,3]. From this figure it can be seen, that the ratio $R_{\bar{p}}$ for small angles θ goes through the maximum $R_{\bar{p}\,max} = 3\times10^{-2}$ at $P = 13$ GeV/c.

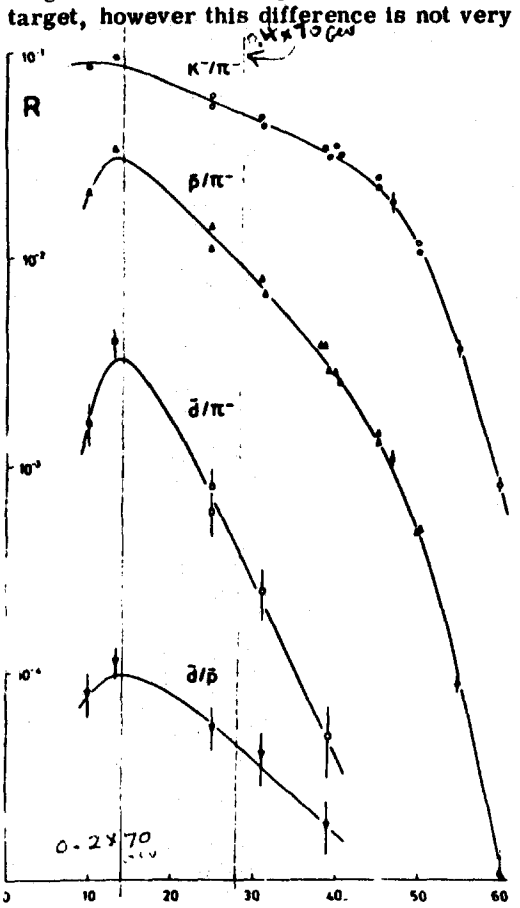

Fig. 1. Relative yields R of kaons, antiprotons and antideuterons, produced in p-Al and p-Be collisions at $E_0 = 70$ GeV. P equals the momentum of the secondaries. Dark pions are the results of the present paper, light points are the data [1-3]. The curves were drawn by hand.

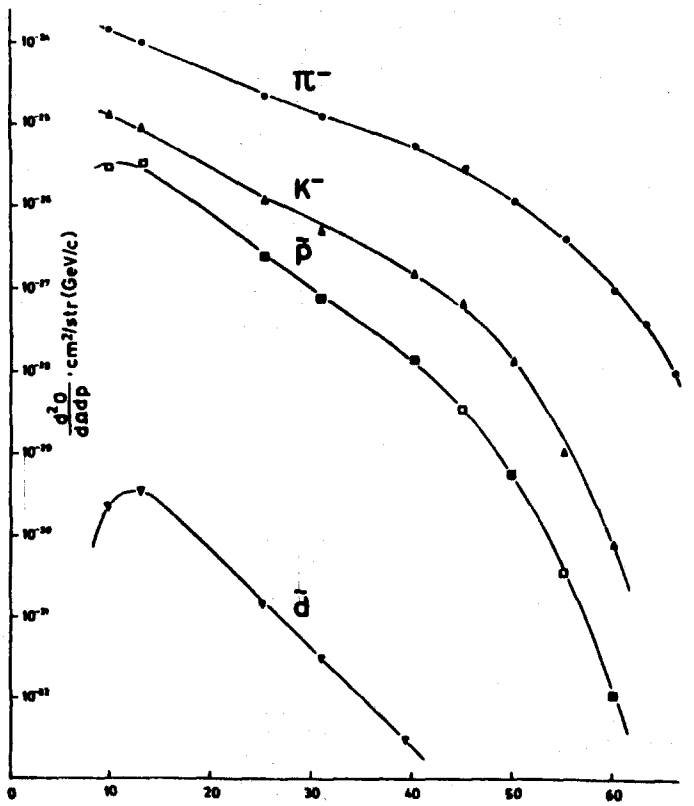

Fig. 2. Differential cross-sections for pion, kaon, antiproton and antideuteron production with momentum P in p-Al collisions at $E_0 = 70$ GeV. Dark points are cross-sections, measured at $\theta = 0^0$. Light points were obtained by cross-section extrapolation to $\theta = 0^0$ (see the text). The curves were drawn by hand.

FIGURE 3

APPENDIX I